PAPER

Check for updates

Synthesis and photophysical properties of (post-)functionalized BOAHY dyes with strong aggregation-induced emission†

Jonathan B. F. Vandenwijngaerden, [iD] ‡[a] Jianjun Huang, [iD] ‡[b] Charlotte Cresens, [iD][a] Wim Dehaen, [iD][b] Luc Van Meervelt, [iD][c] Susana Rocha, [iD][a] Mark Van der Auweraer [iD][a] and Eduard Fron [iD] *[ad]

A series of new difluoroboronate anchored acylhydrazone (BOAHY) derivates were prepared in good yields *via* a simple two-step reaction starting from commercially available reagents. The spectroscopic properties of these dyes can be easily tuned through appropriate functionalization and post-functionalization. While these BOAHYs are dim in solution, they are intensely fluorescent in the solid state, with absolute quantum yields up to 33%. By changing the solvent composition to reduce their solubility, the dyes form aggregates, thus switching on the fluorescence. Steady-state and time-resolved spectroscopy, as well as X-ray crystallography, provide a full characterization of these new BOAHYs and reveal the mechanism behind their aggregation-induced emission (AIE) behavior.

Introduction

Fluorescent molecules have been of interest to scientists for almost two centuries. G. G. Stokes studied the naturally occurring fluorophore quinine and was the first to correctly explain its behavior in terms of the absorption and emission of light, coining the term 'fluorescence' in 1852.[1] The following decades saw the preparation of many types of new synthetic fluorophores. Among them, the organoboron dyes have attracted much attention in recent years because of their structural versatility, tunable photophysical properties, large absorption coefficient, high fluorescence quantum yield, good photostability and simple synthesis.[2] Organoboron dyes consist of a π-conjugated organic core that chelates one or more difluoroboron (BF_2) units. Without the difluoroboron group, excitation of the flexible organic core is mainly followed by non-radiative relaxation to the ground state. Introducing a difluoroboron unit causes the conjugated

π-system to become more rigid and planar, which allows the molecule to relax through the emission of fluorescence photons.[3,4] Furthermore, owing to its strong electron-withdrawing effect, the difluoroboron group can facilitate intramolecular charge transfer (ICT), leading to small bandgaps and long absorption and emission wavelengths.[4–8] The benefits of incorporating this difluoroboron moiety have fueled the development of a multitude of organoboron compounds, including BODIPY,[2,9,10] BOPAHY,[11–13] BOPHY[14,15] and BOPPY[16] derivatives (Fig. 1). Applications such as light harvesting, optoelectronic devices, chemical sensing, biological imaging and medical theranostics have been reported for these dyes.[2,8,10–16]

However, the practical use of organoboron dyes in these fields is often limited by their weak emission in the solid state. While the rigid, planar organoboron core permits intense fluorescence in dilute solutions, this geometry also enables the dye molecules to pack tightly in aggregates or in the solid state. In such a tight packing the excited state is split by exciton interaction and, depending upon the exact packing geometry, the radiative transition from the lowest exciton state is often forbidden.[17–20] This generally leads to a strong reduction of the fluorescence quantum yield. Strong intermolecular π–π stacking interactions between the aromatic rings of neighboring molecules sometimes enable fast non-radiative relaxation of the fluorophore after excitation and therefore further quench the fluorescence.[4,5,21–24] In order to remedy these issues, on can try to prevent aggregation by improving the solubility of the dyes or by fine control of the concentration. Still, such efforts fail to make the dyes suitable for applications in film or solid

[a] *Molecular Imaging and Photonics, Department of Chemistry, KU Leuven, Celestijnenlaan 200F, 3001 Leuven, Belgium*

[b] *Sustainable Chemistry for Metals and Molecules, Department of Chemistry, KU Leuven, Celestijnenlaan 200F, 3001 Leuven, Belgium*

[c] *Biochemistry, Molecular and Structural Biology, Department of Chemistry, KU Leuven, Celestijnenlaan 200F, 3001 Leuven, Belgium*

[d] *KU Leuven Core Facility for Advanced Spectroscopy, Celestijnenlaan 200F, 3001 Leuven, Belgium. E-mail: eduard.fron@kuleuven.be*

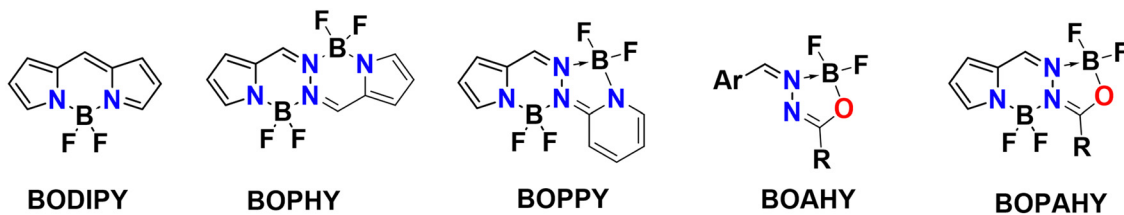‡ J. B. F. V. and J. H. are joint first authors.

Fig. 1   Reported molecular structures of organoboron complexes.

state. In this case, proper substitution of the dye must lead to a packing where the transition from the lowest exciton state to the ground state is enhanced rather than forbidden as is the case in *e.g.* J-aggregates.[25–32] For flexible chromophores where internal rotations in the conjugation chain can lead to rapid non-radiative deactivation,[33–36] the fluorescence intensity can even be enhanced upon aggregation, as intra- and intermolecular interactions within the aggregates restrict vibrational and rotational motion, thus rigidifying the fluorophore and blocking non-radiative decay. The phenomenon that some molecules show strong fluorescence in the solid state, while their emission in dilute solution is relatively weak, was already described by Stokes in 1853.[37] In the 1930s, Scheibe and Jelley were the first to report the emergence of a strong new band in the fluorescence spectrum of molecular aggregates, which was different from the monomer emission band.[25,29,38,39] The new band and the increased fluorescence were correctly attributed to a combination of superradiance and rigidification induced by aggregation. Since 2001, this has been labelled 'aggregation-induced emission' (AIE).[40–43]

Recently, a new family of AIE-active organoboron fluorophores, known as difluoroboronate anchored acylhydrazones (BOAHY), was designed by Jiao and coworkers.[7] BOAHY dyes contain one difluoroboron unit through N–B–O chelation. As such, these compounds are the monochelated form of the BOPAHY dyes, which coordinate two difluoroboron groups through an unsymmetrical combination of N–B–N and N–B–O bridges and which were investigated earlier by both our group as well as Jiao's.[11–13,44] In this context, a series of new BOAHY derivates are presented here. Almost nonfluorescent in

solution, these dyes show considerable fluorescence in the solid state, with fluorescence quantum yields up to 33%. This work reports the synthesis and post-functionalization of these new BOAHY dyes and provides an in-depth photophysical characterization in view of their AIE properties.

## Results and discussion

Synthesis of the BOAHY derivates

BOAHYs **2a–2e** were synthesized started from condensing 2-formyl pyrrole and carbohydrazide in ethanol with the assistance of acetic acid as catalyst (Scheme 1). The formed intermediate hydrazone ligand was subsequently deprotonated using triethylamine, followed by boron chelation in dry toluene to afford the desired BOAHY dyes. For instance, the simplest BOAHY compound, 3,5,7-trimethyl BOAHY **2a**, was obtained with a yield of 55%. BOAHY **2b**, featuring a 4-pyridyl substituent on the oxadiazaborole ring, was synthesized from 3,5-dimethyl-1*H*-pyrrole-2-carbaldehyde and pyridine-4-carbohydrazide, achieving an overall yield of 80%. Compound **2c**, a *meso*-substituted BOAHY dye with a furan moiety at the 3-position, was synthesized with a yield of 78%, by introducing a five-membered heteroaromatic ring substituents. Halogenated BOAHYs **2d** and **2e** were obtained with yields of 60% and 25%, respectively, by utilizing bromohetaryl-substituted hydrazides and 2-formylated 3,5-dimethylpyrrole.

Notably, post-functionalized BOAHYs **2f** and **2g** (as shown in Scheme 2) were efficiently derived from **2d** and **2e**, which possess a bromide functional group. The structures of all
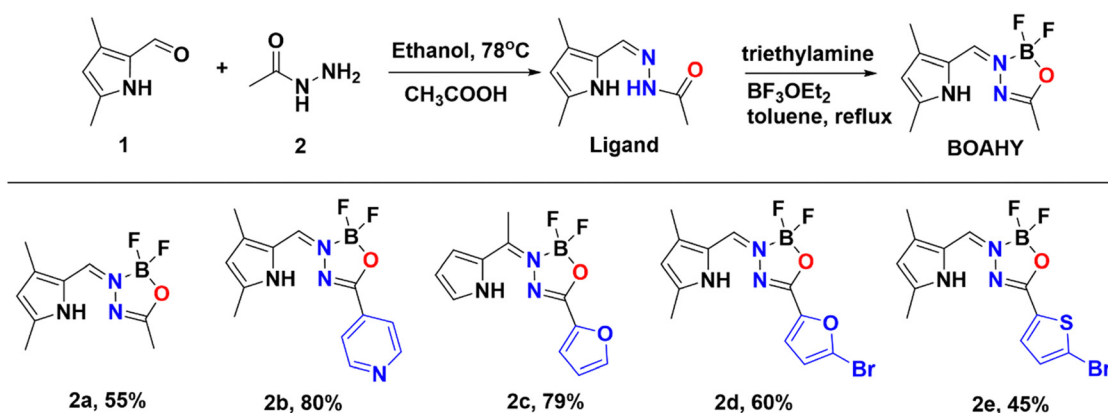
Scheme 1   Synthesis of BOAHYs **2a–2e**.
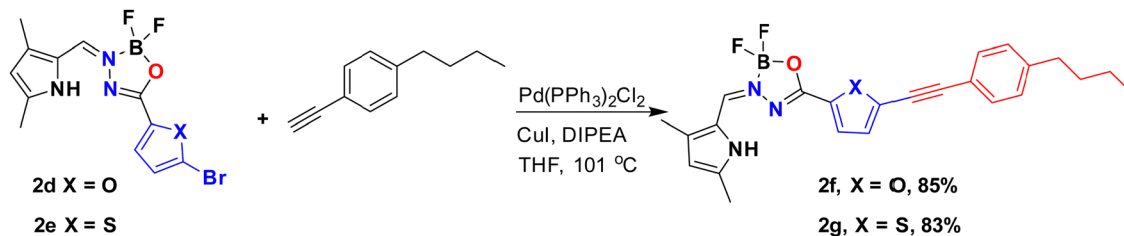
Scheme 2 Synthesis of BOAHYs **2f**–**2g** *via* post-functionalization.

compounds **2a**–**2g** were confirmed through high-resolution mass spectrometry and various NMR spectroscopic techniques including ^1H, ^{11}B, ^{13}C, and ^{19}F NMR spectroscopy, most of them were further confirmed by single X-ray crystallography (see ESI†).

X-ray crystallography

The molecular and crystal structure of compounds **2a**–**2g** was determined by single-crystal X-ray diffraction (Fig. 2, Fig. S1–S7 and Tables S1–S4, ESI†).

Crystals of **2a** were obtained from DCM/pentane and belong to space group $P\bar{1}$. The dihedral angle between the two rings is $9.39(15)°$. In addition to an intramolecular N–H···N hydrogen bond [H10···N4 = 2.27(3) Å], two C–H···F interactions are observed in the crystal packing [H14A···F6^i = 2.54 Å and H16A···F7^{ii} = 2.50 Å; symmetry codes: (i) $1 + x$, $-1 + y$, z, (ii) $1 - x$, $1 - y$, $2 - z$].

Crystals of **2b** were obtained from DCM/pentane and belong to space group $P\bar{1}$. The central ring makes a dihedral angle of $6.13(13)$ and $1.77(11)°$ with the pyrrole and pyridine rings, respectively. An intramolecular N–H···N hydrogen bond [H10···N4 = 2.34(2) Å] helps to extend the conjugation and planarity. The crystal packing is characterized by formation of inversion dimers through C–H···N, C–H···F and π–π stacking interactions. Dimers stacked in columns along the *a*-direction [*Cg*2···*Cg*3^i = 3.7255(14) Å; *Cg*2 and *Cg*3 are the centroids of the pyrrole and pyridine rings; symmetry code: (i) $-x$, $1 - y$, $1 - z$].

Compound **2c** crystallizes from DCM/pentane in space group $P2_1/c$ with two molecules (A and B) in the asymmetric unit. In molecule A the dihedral angles between the central ring

and the pyrrole and furane rings are 4.93(14) and 4.30(14)°, respectively, while 6.30(13) and 3.59(17)° in the other molecule B. In addition to the intramolecular N–H···N hydrogen bonds [H14···N3 = 2.17 Å and H33···N22 = 2.20 Å] also intramolecular C–H···F interactions are present between the methyl group and one of the fluorine atoms [H12A···F18 = 2.53 Å and H31A···F37 = 2.46 Å]. Both molecules are linked by an N–H···F interaction [H33···F19^i = 2.46 Å; symmetry code: (i) $-1 + x$, y, z]. This dimer motif is further extended by N–H···F and C–H···O interactions [H14···F38^i = 2.48 Å and H15···O20^i = 2.58 Å] resulting in layers parallel to (002). No real π–π stacking is observed between these layers.

Also compound **2d** crystallizes in space group $P2_1/c$ with two molecules (A and B) in the asymmetric unit (DCM/pentane used as solvent). Compared to **2c**, the removal of the *meso*-methyl and introduction of bromo (on the furane) and methyl substituents (on the pyrrole) reduces the planarity of the molecule [dihedral angles between central ring and pyrrole and furane rings: 14.6(2) and 0.6(2)° for molecule A, 10.7(2) and 9.95(18)° for molecule B]. The usual intramolecular N–H···N interactions are observed [H14···N3 = 2.29(3) Å and H35···N24 = 2.17(4) Å]. Two types of dimers resulting from C–H···Br interactions are present in the crystal packing (Fig. S4, ESI†): C19–H19C···Br11 for the A–A inversion dimer, C19–H19B···Br32 and C40–H40B···Br11 for the A–B dimer. This dimer formation also leads to π···π stacking and Br···π interactions [*Cg*3···*Cg*5^i = 3.4587(17) Å and Br32···*Cg*3^{ii} = 3.8551(13) Å; *Cg*3 and *Cg*5 are the centroids of pyrrole ring N14 and furane ring O28; symmetry codes: (i) $1 - x$, $-1/2 + y$, $3/2 - z$, (ii) $1 - x$, $1 - y$, $1 - z$].
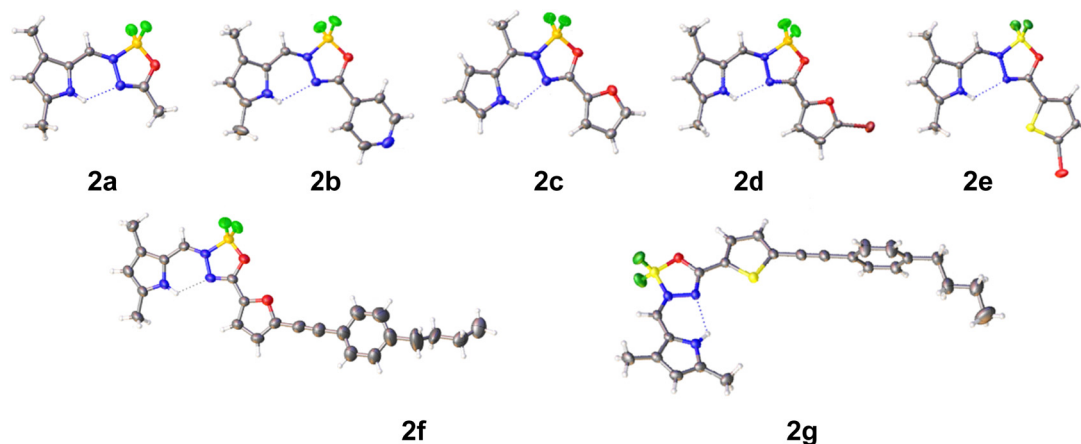
Fig. 2 X-ray crystal structures of **2a**–**2g** with thermal ellipsoids at 30% probability level.

Compound **2e** crystallizes from DCM/pentane in space group $P2_12_12_1$. The introduction of bromo and methyl substituents has no influence on the planarity of the molecule [dihedral angles between central ring and pyrrole and thiophene rings: 2.4(2) and 4.8(2)°]. Again, an intramolecular N–H···N hydrogen bond [H14···N3 = 2.23(4) Å] is present. In contrast to **2c** and **2d**, the thiophene S atom is turned away from the O atom in the central ring (s-trans). The crystal packing shows mainly interactions with the thiophene ring [H9···Cg1^i = 2.84 Å; Cg1 is the centroid of the thiophene ring; symmetry code: (i) 1/2 + x, 3/2 − y, 1 − z] and pyrrole ring [Br11···Cg3^{ii} = 3.3538(18) Å; Cg3 is the centroid of the pyrrole ring; symmetry code: (ii) 2 − x, 1/2 + y, 1/2 − z].

Compound **2f** crystallizes from DCM/diethyl ether in space group $P\bar{1}$. The phenyl-butyl chain is disordered over two positions with occupancies 0.497(11)/0.503(11) for parts 1 and 2, respectively. Additional constraints on bond distances, angles, planarity and temperature factors were necessary for the disordered parts. The dihedral angles between the central ring and the pyrrole and furan rings are 9.2(3) and 3.6(3)°. An intramolecular N–H···N hydrogen bond is observed on both molecules [H25···N3 = 2.25 Å]. The orientation of the furan ring with respect to the central ring is similar to **2d**. The furan ring is inclined by 14.1(7) and 74.9(8)° to the phenyl ring in part 1 and 2, respectively. The shortest Cg···Cg contact is between two pyrrole rings [Cg2···Cg3^i = 3.699(3) Å; Cg2 and Cg3 are the centroids of the furan and pyrrole ring, respectively; symmetry code: (i) 2 − x, 1 − y, −z].

Compound **2g** crystallizes from DCM/pentane in space group $P\bar{1}$ with two molecules (A and B) in the asymmetric unit. The butyl chain in molecule B is disordered over two positions with occupancies 0.464(11)/0.536(11). Both molecules differ in the orientation of the butyl chain (rms deviation overlay of both molecules is 0.5969 Å). In molecule A the dihedral angles between the central ring and the pyrrole and thiophene rings are 9.47(19) and 6.68(18)°, respectively, while 9.7(2) and 6.61(19)° in the other molecule B. An intramolecular N–H···N hydrogen bond is observed on both molecules [H25···N3 = 2.26(3) and H57···N35 = 2.27(3) Å]. The orientation of the thiophene ring with respect to the central ring is similar to **2e**. Both thiophene rings are involved in C–H···π interactions [H15···Cg5^i = 2.82 Å, H49···Cg1^i = 2.87 Å; Cg5 and Cg1 are the centroids of the thiophene rings in molecules A and B, respectively; symmetry code: (i) x, −1 + y, z]. In addition, C–H···F interactions are present between neighboring molecules [H29B···F32^{ii} = 2.55 Å, H61A···F63 = 2.50 Å; symmetry code: (ii) 1 + x, −1 + y, z]. The shortest Cg···Cg contact is between two pyrrole rings [Cg3···Cg3 = 3.700(2) Å; Cg3 is the centroid of the pyrrole ring in molecule B; symmetry code: (iii) 2 − x, 1 − y, −z]. None of the crystal packings shows the presence of voids.

Steady-state spectroscopy in solution and solid state

The steady-state absorption and emission spectra of BOAHYs **2a–2g** were measured in acetonitrile, heptane (2.0 × 10^{-5} mol L^{-1}) and the solid state, in order to evaluate how their molecular structure and functional groups affect their photophysical properties. Fig. 3 shows the normalized absorption

and emission spectra measured in solution. The corresponding spectra of solid powders are provided in the ESI† (Fig. S11, ESI†). The important spectroscopic data are listed in Table 1.

Having only methyl groups as substituent on its oxadiazaborole ring, **2a** is used here as reference to which the other functionalized and post-functionalized compounds can be compared. In acetonitrile, **2a** has a strong absorption band around 354 nm with a relatively large molar extinction coefficient of 3.5 × 10^4 L mol^{-1} cm^{-1}, which is in agreement with values reported earlier for similar dyes.[44] Besides the maximum at 354 nm, which can be attributed to the $v_0'' \rightarrow v_1'$ band of the $S_0 \rightarrow S_1$ ($\pi \rightarrow \pi^*$) transition, the spectrum exhibits a shoulder around 366 nm corresponding to the $v_0'' \rightarrow v_0'$ transition (vibrational progression of around 900 cm^{-1}). The absorption spectra of **2b–2g** show an additional vibrational band around 375 nm attributed to the $v_0'' \rightarrow v_2'$ transition (vibrational progression of around 1200 cm^{-1}).

At 287 nm, a weak additional band appears in the spectrum of **2a**, which can be assigned to the S_0–S_1 transition. Such a short-wavelength band around 250–350 nm is present in the absorption spectra of all other compounds and is generally weaker than the S_0–S_1 band, except for the post-functionalized molecules **2f** and **2g** where both bands have nearly the same magnitude.

By changing the substituent on the oxadiazaborole ring, the wavelength of the S_0–S_1 absorption band can be tuned over a spectral range from 366 to 444 nm. For example, inserting a (brominated) aromatic heterocyclic substituent such as a pyridine (**2b**) a furan (**2d**) or a thiophene (**2e**) increases the wavelength of the $v_0'' \rightarrow v_1'$ transition in heptane from 363 nm to respectively 408 nm (**2b**), 386 nm (**2c**), 414 nm (**2d**) or 424 nm (**2e**). As both electron withdrawing (**2b**) or electron donating moieties (**2c** to **2e**) lead to redshift, the effect of the substituent is rather due to an extension of the conjugated system rather than to the enhancement of intramolecular charge transfer. This lowers the HOMO–LUMO gap and causes a redshift of the absorption and emission spectra. Since thiophene has a higher aromaticity than furan, the π-electrons are more delocalized in the conjugated system containing thiophene.[45] Therefore, the shift in absorption wavelength maximum is larger upon substitution with thiophene (424 nm for **2e**) when compared to furan (416 nm for **2d**). Quite surprisingly and in contrast with similar compounds[11–13] the Stokes shift and FWHM of the emission band are not increased upon introduction of this substituent. This indicates very little electron–phonon coupling with rotation of this substituent or a difference in its coplanarity in ground and excited state. Moreover, the bromine functionality opens up synthetic possibilities for post-functionalization strategies, aimed at adding groups that could increase the conjugation length even more. In particular, the introduction of a 4-butyl-phenylacetylene moiety on the furan and thiophene rings resulted in a further redshift of the absorption and emission spectra to respectively 433 nm and 522 nm for **2f** and 444 nm and 505 nm for **2g**, due to a further increase in the size of the conjugated system. For all the investigated dyes, the molar extinction
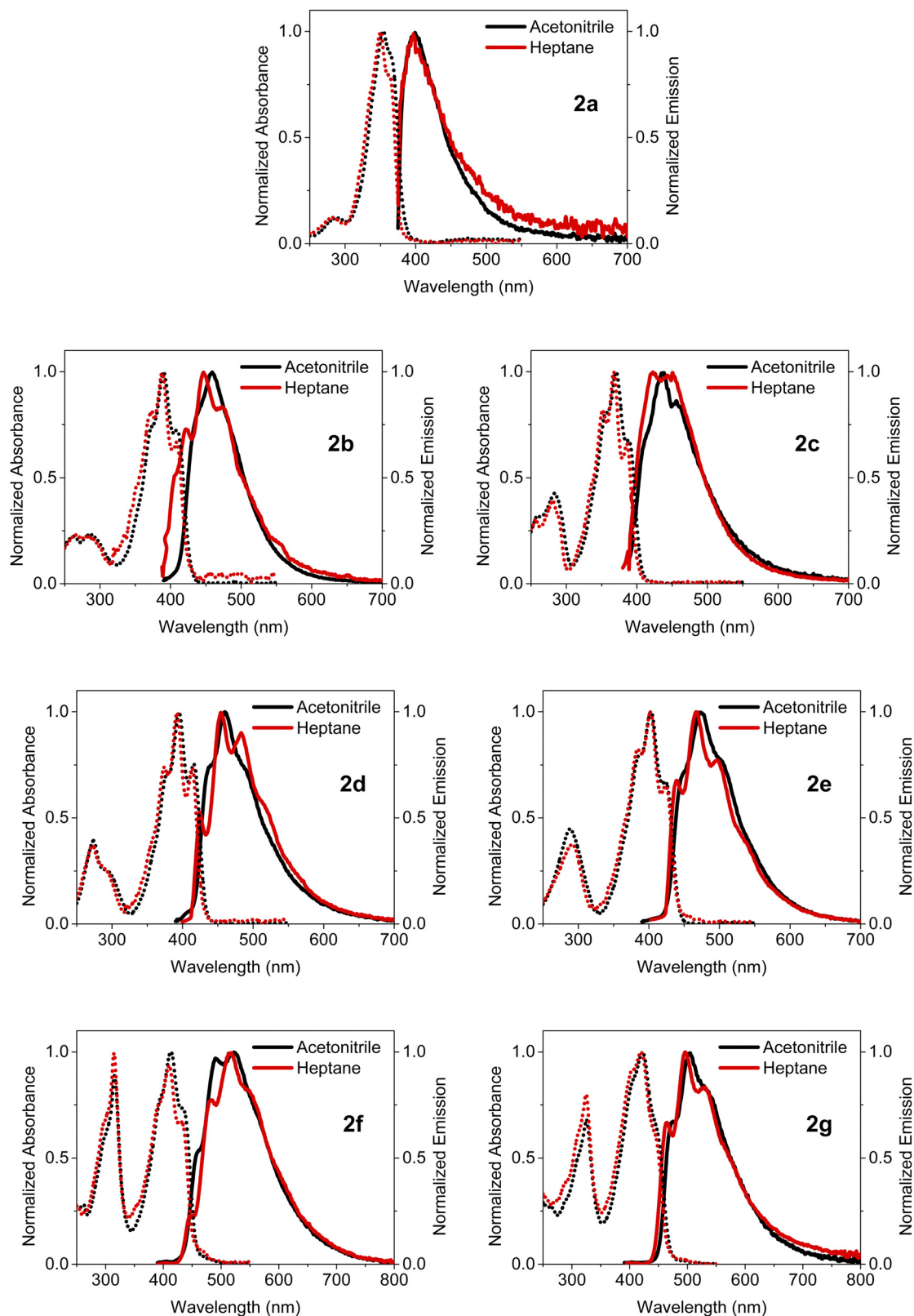
Fig. 3 Normalized absorption and emission spectra of **2a–2g** in acetonitrile and heptane.

coefficients at the absorption maximum range between 3.5 and 5.5×10^4 L mol^{-1} cm^{-1}.

Compared to the absorption spectra in the apolar solvent heptane (with dielectric constant $\varepsilon_R = 1.9$), the absorption

Table 1 Selected spectroscopic properties of **2a–2g** in the solid state and dissolved in acetonitrile, heptane and water/acetonitrile mixture with water fraction $f_w = 0.99$. λ_{abs} is the absorption maximum of $S_0–S_1$ 0–0 band, λ_{em} is the fluorescence emission maximum, $\bar{\nu}_{abs}–\bar{\nu}_{em}$ is the Stokes shift (calculated from the maxima of the absorption and emission spectra), ϕ_F is the absolute fluorescence quantum yield, ε is the molar extinction coefficient at the absorption maximum

Molecule	Solvent	λ_{abs} (nm)	λ_{em} (nm)	$\bar{\nu}_{abs}–\bar{\nu}_{em}$ (cm^{-1})	FWHM$_{em}$ (cm^{-1})	ϕ_F	ε (L mol^{-1} cm^{-1})
2a	Acetonitrile	366	399	3190	3880	<0.01	35 000
	Heptane	363	397	3380	4250	<0.01	
	Solid	476	540	6800	3760	0.01	
	Water/acetonitrile	366	412	3980	3980	<0.01	
2b	Acetonitrile	409	459	3860	3690	<0.01	36 900
	Heptane	408	447	3340	4770	<0.01	
	Solid	510	539	5260	4880	0.21	
	Water/acetonitrile	410	532	6840	4920	0.07	
2c	Acetonitrile	388	438	4120	4650	<0.01	41 800
	Heptane	386	423	3610	4920	<0.01	
	Solid	420	476	4240	3680	0.02	
	Water/acetonitrile	388	446	4460	4730	<0.01	
2d	Acetonitrile	416	460	3580	3800	<0.01	55 000
	Heptane	414	454	3480	3700	<0.01	
	Solid	434	517	3700	2980	0.03	
	Water/acetonitrile	438	517	8750	3880	0.01	
2e	Acetonitrile	424	472	3630	3890	<0.01	38 700
	Heptane	424	468	3510	3880	0.01	
	Solid	437	527	3910	2830	0.04	
	Water/acetonitrile	446	495	6320	3000	0.05	
2f	Acetonitrile	433	522	5060	4890	<0.01	42 200
	Heptane	430	513	4900	4360	0.02	
	Solid	502	572	6970	3010	0.33	
	Water/acetonitrile	452	563	5940	3850	0.18	
2g	Acetonitrile	444	505	3840	4100	0.03	45 000
	Heptane	443	496	3650	4480	0.07	
	Solid	502	575	6590	3420	0.24	
	Water/acetonitrile	456	570	8840	4070	0.16	

spectra of all compounds in the more polar solvent acetonitrile ($\varepsilon_R = 37.5$) are modestly redshifted over 0 to 226 cm^{-1}. This could indicate that the BOAHY molecules have a modest ground state dipole moment and are slightly more polar in the excited state than in the ground state. To accurately determine the dipole interaction one needs to consider the larger polarizability of heptane relative to acetonitrile, an effect that induces an additional redshift as *e.g.* observed for BODIPY dyes.[2,46]

The emission spectra show, with exception of **2b** and **2c**, a redshift of 130 to 360 cm^{-1} from heptane to acetonitrile indicating a very small or absent dipole moment in the ground state and a small dipole moment in the S_1 excited state. **2b** and **2c** show a larger redshift of respectively 590 and 810 cm^{-1} indicating a larger excited state dipole moment. As already mentioned for the absorption spectra, the observed shift underestimates the dipolar interactions as the larger polarizability of heptane normally induces a redshift from acetonitrile to heptane which has been observed for BODIPY dyes.[2,46] The emission spectra of the dyes in acetonitrile and heptane feature a Stokes shift of 3190–5060 cm^{-1}, which is substantially larger than the few hundreds of cm^{-1} typically reported for BODIPY dyes. This agrees with the observation that while for most

BODIPY dyes[2] the $v_0'' \to v_0'$ or $v_0' \to v_0''$ vibronic bands are the most intense transitions in the $S_0 \to S_1$ absorption band and in the fluorescence spectrum this is here the case for the $v_0'' \to v_1'$ or $v_0' \to v_1''$ vibronic bands. The relative large Stokes shift and FWHM of the emission spectra are mainly related to electron–phonon coupling with the high frequency vibration of about 900 cm^{-1} (cfr. infra) rather than to coupling with low frequency vibration such a torsions around the conjugates system. This indicates that there is little change in planarity upon excitation. On the other hand, the changes in equilibrium bond length of the conjugated system are substantial for the BOAHY dyes. While the fluorescence band of **2a** is structureless in solution, the emission spectra of some of the other compounds show vibronic maxima which are the mirror-image of the absorption spectra. For example, the emission spectrum of **2d** in heptane has (shoulder) peaks around 424, 454, 483 and 520 nm, corresponding to a vibrational progression around 1450 cm^{-1}. To better resolve this vibrational fine structure, the emission spectra of **2d** and **2e** were measured at 77 K in methyltetra-hydrofuran (MeTHF) (Fig. S10, ESI†). The matching excitation spectra prove that the different fluorescence bands originate from the same apparent species.

The fluorescence quantum yields in solution are negligible for compounds **2a–2e** (1% or below) and low for the post-functionalized dyes **2f** and **2g** (7% or below). However, in the solid state, some of these dyes show considerably higher fluorescence quantum yields. This is especially the case for **2b**, **2f** and **2g** which have quantum yields of respectively 21%, 33% and 24% in the solid state, several times the multiple of their values in acetonitrile.

In order to elucidate the mechanisms behind the fluorescence quenching in solution and the amplification of fluorescence in solid state, the excited state dynamics of the BOAHYs were further examined by means of time-resolved spectroscopy. The fluorescence decays were determined in acetonitrile, a water acetonitrile mixture ($f_w = 0.99$) and in the solid state using time correlated single photon counting (TC-SPC) and (only for acetonitrile) femtosecond fluorescence up-conversion (fsUC) (Fig. 4 and Tables S5, S6, ESI†). A scheme showing the main photophysical processes involved in the relaxation is presented in Fig. 5. The TC-SPC and fsUC decays were fitted to a double or triple exponential decay. For solutions of **2a** to **2f**, the fluorescence decay at room temperature is beyond the time resolution of TC-SPC, the low amplitude nanosecond decay components probably being due to impurities. These experiments are confirmed by the fsUC experiments which show for
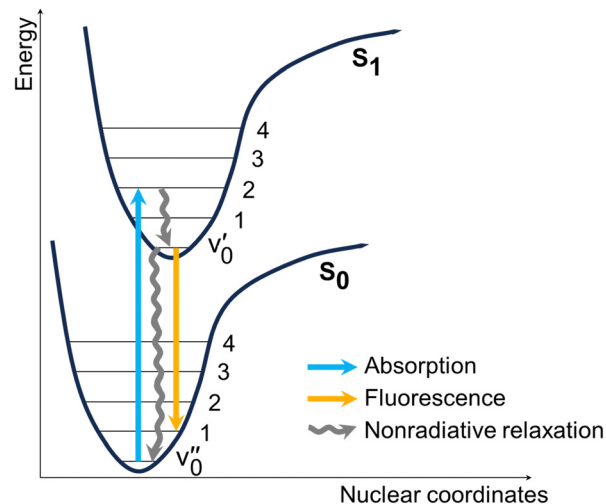

Fig. 5 Generic scheme showing the photophysical processes that occur upon excitation of the dyes. Nonradiative relaxation includes both vibrational and rotational decay channels.

2a a fluorescence decay time of about 2 ps and for **2b** to **2f** decay fluorescence decay times between 9 and 45 ps. Besides these components, the faster ones observed as rise and decay of
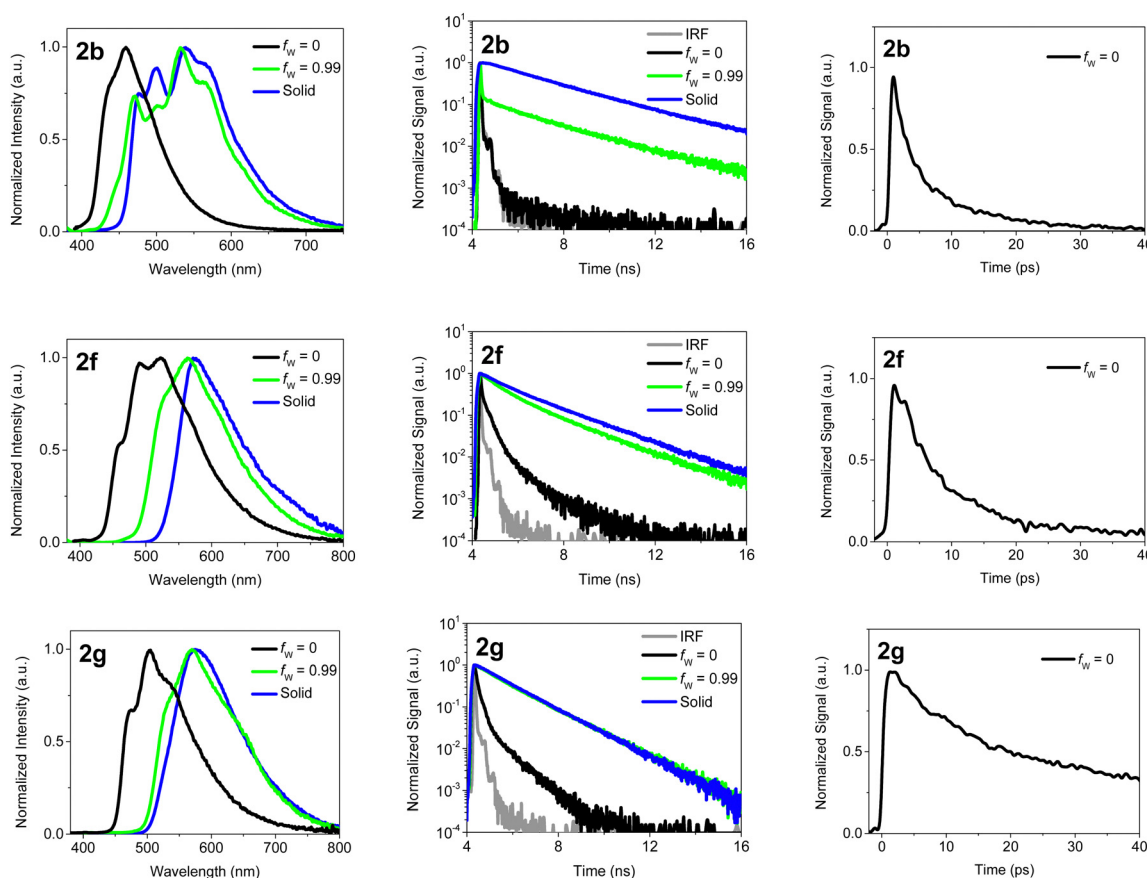

Fig. 4 Left: Normalized emission spectra of **2b**, **2f** and **2g** in solid state and solved in water/acetonitrile with water fractions $f_w = 0$ and 0.99, excited at 360 nm. Middle and right: Corresponding fluorescence decays of **2b**, **2f** and **2g**, excited at 360 nm and detected at 530 nm, measured with TC–SPC (middle) and fsUC (right, only acetonitrile).

fluorescence signal in the 0–1000 fs time window can be attributed to intramolecular vibrational relaxation of vibrational redistribution.[47] Such ultrafast components have also been observed earlier in other BODIPY compounds via 2D electronic spectra and DFT calculations and attributed to solvation dynamics and vibrational modes strongly coupled to the electronic excitation.[48] The time components reported in Table S6 (ESI†) with values of 1–8 ps suggest processes leading to severe depopulation of the S_1 state as they feature large and positive relative amplitudes.

These fast decays are the main reason for the low fluorescence quantum yields in solution as based on the molar extinction coefficients (Table 1), which resemble those of BODIPYs,[2,46] similar fluorescence rate constants in the order of a few times 10^8 s^{-1} can be expected. For **2f** and **2g** the longer fluorescence decay times of 120 and 61 ps, as determined by fsUC, are compatible with the larger fluorescence quantum yields.

Fig. 4 shows the emission spectra of **2b**, **2f** and **2g** in water/acetonitrile mixtures and in the solid state together with the corresponding fluorescence decays measured with TC-SPC or fsUC. Additional data for the other compounds can be found in the ESI† (Fig. S24, S25 and Tables S5, S6, ESI†). Compared to the spectra in acetonitrile the fluorescence spectra in the solid state are redshifted over 1820 cm^{-1} (**2c**) to 3230 cm^{-1} (**2b**) and even 6540 cm^{-1} for **2a**. This shift can be attributed to intermolecular interactions which are partly due to exciton interaction.[17–20,27,28,31]

In contrast to what is generally observed for emission of molecular aggregates, the aggregate emission spectra still show some vibrational structure for **2b** and **2e**, and less outspoken for **2a**, **2c** and **2d**. For **2b** and to a smaller extent for **2a** also fluorescence which resembles that of the dye monomers although redshifted over about 1000 cm^{-1} is still observed in the solid state. The absorption maxima of **2a** to **2e** are redshifted by 1000 to 2000 cm^{-1} and for **2f** and **2g** this shift is increased to respectively 3200 and 2600 cm^{-1}. Furthermore the absorption spectra of **2a** and **2b** have a shoulder which is redshifted by respectively 4800 and 6300 cm^{-1}.

For **2a** to **2f** the majority of the molecules is packed in such way that the exciton interaction leads to a redshift of 1000 to 3000 cm^{-1} for the absorption spectra and 1500 to 2500 cm^{-1} for the emission spectra. This means a packing similar to J-type aggregates for which emission from the lowest exciton state is allowed.[17–20,27,28,31] For **2a** and **2b** a small fraction of the molecules form J-type aggregates where stronger intermolecular interactions lead to a redshift of the absorption by respectively 6300 and 4800 cm^{-1} while the emission is redshifted by 6500 and 3400 cm^{-1}. While the absorption spectra indicate that only a small fraction of the dye molecules adopts this packing, these redshifted aggregates give a major contribution to the emission spectra. This suggests the occurrence of energy transfer between both types of aggregates.

Upon visual inspection, the fluorescence decays in the solid state are much slower than those in acetonitrile. Although the decays could be fitted to a bi- or tri-exponential decay, one

should, in the absence of a kinetic scheme leading to such decays, realize that this fitting is not unique and that the decays could probably as well be fitted to a stretched exponential or a distribution of decay times.[49,50] Therefore, in this case most individual decay times and their amplitudes have no physical meaning, except for the longest time component τ_3 which can be interpreted as a lower limit for the decay time of the molecules. Besides a distribution over a range of packings leading to different decay rates, one should consider that such non-single-exponential luminescence decays of solids are often governed by energy transfer to non-fluorescent traps.[22,23,50–56] In this case the longest decay time approaches the fluorescence decay time of the unquenched aggregates. The latter decay times ranging from 1.18 ns to 4.71 ns are 10 to 1000 times larger than those in acetonitrile. As this increase in decay time is accompanied by an increase of the fluorescence quantum yield, the non-radiative decay must be much slower in the solid state compared to the solution in acetonitrile. Since the non-radiative decay rate of BOAHY dyes is heavily influenced by viscosity,[7] a possible explanation for such long decay times in the solid state could be the rigidification of the environment of the dyes. The rotations around the partial double bonds, which are mainly responsible for the fast non-radiative decay, are blocked due to the close packing of the dyes in the solid state, which causes longer decay times. To check that rotations are the main reason for the fluorescence quenching in solution at room temperature, the fluorescence decay of **2b** in acetonitrile at 77 K was measured with TC-SPC. At this low temperature, most thermally activated rotations are blocked, leading to a fluorescence decay that is very similar to the one measured in solid state, with a long decay time of 2.94 ns (Fig. S24, ESI†). Hence, the BOAHYs in solution at room temperature lose most energy in a non-radiative way after excitation, probably via free rotations of the unchelated pyrrolic rings. The suppression of these rotations due to rigidification in the solid state cause the high fluorescence quantum yields of the solid powders compared to the solutions. When one compares spectra and fluorescence decay times of BOAHYs with the aryl substituted BOPAMs[57] or BOPAHYs[11] the generally much faster nonradiative decay of the BOAHYs is not reflected systematically in a significantly broader spectra or a significantly larger Stokes shift. This indicates that this pyrrole nucleus has a similar degree of coplanarity in the ground and excited state, perhaps related to H-bonding between the pyrrole NH and a nitrogen atom of the hydrazone moiety. In this case the rotation of the pyrrole is only an inducing and not an accepting mode for the internal conversion to the S_0 state.[58]

Aggregation in water/acetonitrile mixtures

Stimulated by the stronger fluorescence in solid state, we investigated whether the emission of BOAHYs **2a–2g** could be switched on by adjusting the solubility and inducing aggregation. To this end, mixtures of acetonitrile (good solvent) and water (non-solvent) were used to control the dissolution and aggregation of the fluorescent molecules. The steady-state absorption and emission spectra of **2a–2g** in mixtures with

different volumetric water fractions (f_w) between 0% and 99% are available in the ESI† (Fig. S14–S20, ESI†). Some figures of merit for the solutions with the highest water fraction (f_w = 0.99) are included in Table 1.

For the methyl-substituted BOAHY **2a**, neither the absorption spectrum nor the emission spectrum change much with increasing f_w and the expected accompanying reduction of the solubility. The position of the S_0–S_1 0–0 absorption band is the same for 99% water as for pure acetonitrile. While the emission spectrum retains approximately the same shape and intensity, its maximum is slightly redshifted, which considering the small excited state dipole moment can be related to an increased polarity of the environment. The quantum yields are low in all water/acetonitrile mixtures and show only a small increase to 0.01 in the solid state. The same observations hold for **2c**, with exception that for f_w = 99% the absorbance is now reduced by about 50%. Thus, enhancing the emission by inducing aggregation could not be achieved for BOAHYs **2a** and **2c**.

For f_w = 99% the fluorescence spectra of **2b** and **2d–2g**, nicely coincide with the solid state emission spectra (Fig. 4 and Fig. S15, S17–S20, S22, ESI†). A similar behavior is observed for the fluorescence quantum yields which are, although several times larger than in neat acetonitrile, with exception of **2e** still smaller than in the solid state (Table 1). The latter can perhaps be due presence of water enhancing the local polarity. Looking in more detail (Fig S15–S20, ESI†) a gradual shift of the spectra can be observed. When gradually increasing the water fraction, the emission intensity first decreases, probably due to an increased polarity enhancing quenching by intramolecular charge transfer. Above *circa* 70–80% water (40% water for **2g**), the fluorescence quantum yield greatly increases while the emission spectrum shifts to longer wavelengths (Fig. S23, ESI†). Fig. S23 (ESI†) also shows that the water content where the intensity starts to be enhanced increases in the order **2g** < **2f** < **2e** < **2b** < **2d** which follows a decreasing hydrofobicity of the BOAHY dyes. Also the water content where the switch in the features of the emission spectra is observed (Fig. S15 and S17–S20, ESI†) follows the same order. This means that the onset of the spectral shift and the increase of the intensity is linked to onset of the precipitation of the BOAHY dyes. Also the absorption spectra (Fig. S15 and S17–S20, ESI†) are characterized by a loss of structure, a spectral broadening and a redshift of the S_0–S_1 0–0 absorption band for higher water contents.

These findings from steady-state spectroscopy clearly point out that with decreasing solubility, molecular aggregates are formed for these BOAHYs which even precipitate at the highest water content leading to a turbity of the solutions (Fig. S21, ESI†). This behavior is particularly prominent for **2b** with pyridine substituent and the post-functionalized dyes **2f** and **2g**. In these aggregates, the strong dipole–dipole interactions together with the rigidification of the fluorophore give rise to an impressive increase of fluorescence intensity, which is the hallmark of the AIE effect. Because of the very fast (picosecond or subpicosecond) vibrational relaxation to the lowest excited exciton level after excitation, the aggregate emits at longer wavelengths in comparison to the monomer.

To verify the formation of aggregates with increasing water fraction and to better understand the excited state processes in the aggregates, the fluorescence decays were studied with TC-SPC. From Fig. 4 (and Fig S24, ESI†) it is clear that for the water/acetonitrile mixture with 99% water, the fluorescence decays of **2b** and **2d–2g** are significantly slower than in pure acetonitrile and start to resemble those of the solid state dyes. Especially, the fluorescence decay of **2f** and **2g** in the water/acetonitrile mixture (with long decay times of respectively 2.29 ns and 1.67 ns) is remarkably parallel to the decay of the solid powder (with long decay times of respectively 2.20 ns and 1.52 ns). For **2b** the same is also observed at longer times, suggesting that we have here still a mixture of solid **2b** and molecules of **2b** in solution. For **2d** and **2e** the fluorescence decays although slower than in neat acetonitrile are still faster that in the solid state. This indicates that for f_w = 99% not yet the solid phase is formed but rather small aggregates of **2d** and **2e**. The latter is also reflected in the emission spectrum of **2e** which for f_w = 99% still different from that in the solid state. In aggregates and in the solid state, the close packing of the dye molecules hinders the free rotations, leading to a decrease of the non-radiative decay rate and a longer decay time, much like in the solid state. Hence, these long decay times further corroborate that the BOAHY dyes form aggregates or precipitate in water/acetonitrile mixtures with a high water content.

In contrast to the other compounds the environment of **2a** and **2c** in solutions with a large f_w resembles more that of neat acetonitrile rather than the solid state. Apparently no precipitation or aggregation occurs for **2a** and **2c** indicating a higher solubility of **2a** and **2c** in water, related to a less hydrophobic character. Actually one can try the estimate the hydrophobic character by comparing the number of 2nd or 3rd row elements with the number of the groups (–O–, ═N–, –NH–, BF) that can be involved in hydrogen bonding. This ratio decreases from 6/16 for **2a** over 7/18 for **2c** to 6/32 for **2g**. In fact, the decrease of this ratio parallels the decrease of the value of f_w where the transition from the solution to the solid state spectrum and intensity occurs (Fig. S15, S17–S20 and S23, ESI†).

Compatibility with biological imaging

Finally, the applicability in biological imaging was investigated for BOAHY **2f**, because of its slightly higher fluorescence quantum yield compared to the other studied compounds and since the small dot-like aggregates formed when dissolved in aqueous medium were hypothesized to be most compatible with live-cell imaging (Fig. S26, ESI†). To this end, HeLa cells were incubated with 10 μM BOAHY **2f** for 4 h, excess dye was washed away, and cellular internalization was investigated by staining the cellular membranes using the commercial near-infrared DiR dye.

Fluorescence imaging (Fig. 6) reveals that **2f** is predominantly found intracellularly with respect to the DiR stained plasma membrane after 4 h incubation. We hypothesize that this preferential intracellular build-up is caused by the hydrophobic character of the dye, which enables entrance into the cell, but that the formation of larger aggregates prevents it from
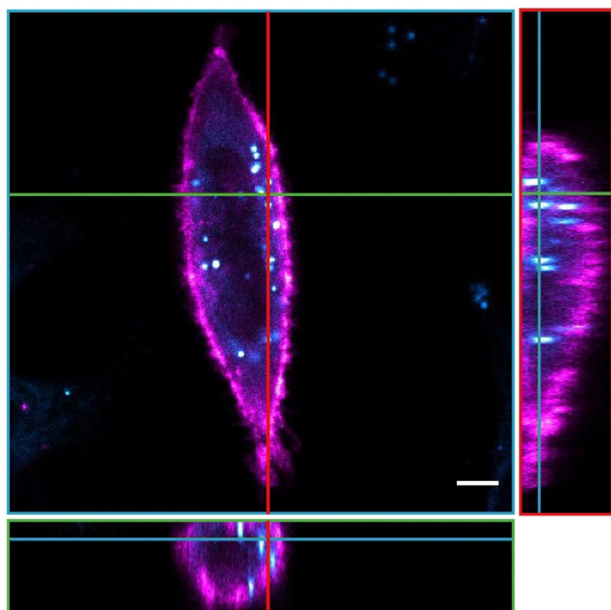
Fig. 6 Fluorescence microscopy image of a HeLa cell incubated with BOAHY dye **2f** (cyan) and stained with DiR membrane stain (pink). The figure displays the cross-section of a cell (blue borders and lines) with orthogonal *YZ* (red borders and lines) and *XZ* (green borders and lines). Scale bar 5 μm.

being released back into the extracellular environment. Note that **2f** was also not localized in the nucleus (which is perceived as a darker structure), probably because this hydrophobic character and size of the dye prevents them from entering through the nuclear pores.[59] Additionally, staining of lysosomes using the commercial LysoTracker™ Deep Red dye revealed that **2f** is not found in lysosomal vesicles after 4 h, but rather seems to be present at intracellular locations where fewer lysosomes are found (Fig. S27, ESI†). In addition, **2f** does not seem to alter cell morphology or induce toxicity in the cells. These experiments illustrate the compatibility of BOAHY dye **2f** with biological imaging in living mammalian cells.

Conclusion and outlook

In conclusion, a set of new BOAHY dyes were synthesized *via* a two-step reaction with good yields. Through proper functionalization and post-functionalization, their photophysical properties such as absorption and emission maxima could be tuned. Since the dyes are dim in solution but brightly fluorescent in the solid state, the properties related to their AIE behavior were thoroughly investigated by means of steady-state well as time-resolved spectroscopy techniques. It was found that the fluorescence could be switched on by changing the solubility of the dyes from good (acetonitrile) to poor (water/acetonitrile with 99% water). In a poor solvent, the BOAHYs form aggregates which causes a broader and redshifted absorption, a more intense redshifted emission, higher quantum yields and longer decay times, relative to the values in acetonitrile.

In comparison to the methyl-substituted compound **2a**, these results are especially outspoken for the pyridine-substituted dye **2b** and for the post-functionalized dyes **2f** and **2g**, the most hydrophobic BOAHY dyes The latter two show improved quantum yields compared to their respective bromine-functionalized analogs **2d** and **2e**. Interestingly, the aggregates of BOAHY **2f** are compatible with living mammalian cells, which opens the possibility of the application of BOAHY dyes as bright fluorescent probes for the visualization of biological samples.

As a continuation of this research, it would be fascinating to explore whether the fluorescence of BOAHY derivates can also be activated by adding metal salts. If selective chelation of a metal cation would induce rigidification of the fluorophore structure, this would allow to use these dyes as ion sensors.

Author contributions

Jonathan B. F. Vandenwijngaerden, Jianjun Huang: conceptualization, investigation, formal analysis, visualization, validation, writing – original draft, writing – review & editing; Charlotte Cresens, Luc Van Meervelt: investigation, formal analysis, visualization, writing – review & editing; Wim Dehaen, Susana Rocha, Mark Van der Auweraer, Eduard Fron: conceptualization, supervision, writing – review & editing.

Conflicts of interest

There are no conflicts of interest to declare.

Acknowledgements

References

1 G. G. Stokes, *Philos. Trans. R. Soc. London*, 1852, **142**, 463–562.

2 N. Boens, B. Verbelen, M. J. Ortiz, L. Jiao and W. Dehaen, *Coord. Chem. Rev.*, 2019, **399**, 213024.

3 H. Lu, J. Mack, Y. Yang and Z. Shen, *Chem. Soc. Rev.*, 2014, **43**, 4778–4823.

4 Y. Yu, C. Yu, Q. Wu, H. Wang, L. Jiao, W. Y. Wong and E. Hao, *J. Mater. Chem. C*, 2019, **7**, 4533–4542.

5 D. Frath, J. Massue, G. Ulrich and R. Ziessel, *Angew. Chem., Int. Ed.*, 2014, **53**, 2290–2310.

6 D. Wang, M. M. S. Lee, G. Shan, R. T. K. Kwok, J. W. Y. Lam, H. Su, Y. Cai and B. Z. Tang, *Adv. Mater.*, 2018, **30**, 1802105.

7 C. Yu, E. Hao, X. Fang, Q. Wu, L. Wang, J. Li, L. Xu, L. Jiao and W. Y. Wong, *J. Mater. Chem. C*, 2019, **7**, 3269–3277.

8 J. Heo, D. P. Murale, H. Y. Yoon, V. Arun, S. Choi, E. Kim, J. Lee and S. Kim, *Aggregate*, 2022, 1–35.

9 A. Treibs and F.-H. Kreuzer, *Justus Liebigs Ann. Chem.*, 1968, **718**, 208–223.

10 F. de Jong, J. Pokorny, B. Manshian, B. Daelemans, J. Vandaele, J. B. Startek, S. Soenen, M. Van der Auweraer, W. Dehaen, S. Rocha and G. Silveira-Dorta, *Dyes Pigm.*, 2020, **176**, 108200.

11 F. de Jong, D. Verhaeghe, K. Veys, J. Huang, W. Dehaen, D. Escudero, E. Fron and M. Van der Auweraer, *Dyes Pigm.*, 2022, **206**, 110662.

12 S. Pookkandam Parambil, F. de Jong, K. Veys, J. Huang, S. P. Veettil, D. Verhaeghe, L. Van Meervelt, D. Escudero, M. Van der Auweraer and W. Dehaen, *Chem. Commun.*, 2020, **56**, 5791–5794.

13 T. Horsten, F. De Jong, D. Theunissen, M. Van Der Auweraer and W. Dehaen, *J. Org. Chem.*, 2021, **86**, 13774–13782.

14 S. Boodts, E. Fron, J. Hofkens and W. Dehaen, *Coord. Chem. Rev.*, 2018, **371**, 1–10.

15 L. I. Shamova, Y. V. Zatsikha and V. N. Nemykin, *Dalton Trans.*, 2021, **50**, 1569–1593.

16 C. Yu, Z. Huang, X. Wang, W. Miao, Q. Wu, W.-Y. Wong, E. Hao, Y. Xiao and L. Jiao, *Org. Lett.*, 2018, **20**, 4462–4466.

17 M. Kasha, *Rev. Mod. Phys.*, 1959, **31**, 162–169.

18 M. Kasha, *Radiat. Res.*, 1963, **20**, 55–70.

19 A. S. Davydov, *Sov. Phys. Uspekhi*, 1964, **7**, 145–178.

20 T. Förster, in *Modern Quantum Chemistry, Part IIIB*, ed. O. Sinaoglu, Academic Press, New York, 1965, pp. 93–137.

21 J. Mei, N. L. C. Leung, R. T. K. Kwok, J. W. Y. Lam and B. Z. Tang, *Chem. Rev.*, 2015, **115**, 11718–11940.

22 K. Kemnitz, T. Murao, I. Yamazaki, N. Nakashima and K. Yoshihara, *Chem. Phys. Lett.*, 1983, **101**, 337–340.

23 F. Willig, A. Blumen and G. Zumofen, *Chem. Phys. Lett.*, 1984, **108**, 222–227.

24 E. G. McRae and M. Kasha, *J. Chem. Phys.*, 2004, **28**, 721–722.

25 E. E. Jelley, *Nature*, 1936, **138**, 1009–1010.

26 L. G. S. Brooker, F. L. White, D. W. Heseltin, G. H. Keyes, S. G. Dent and E. J. Van Lare, *J. Photogr. Sci.*, 1953, **1**, 173–183.

27 V. Czikkely, H. D. Försterling and H. Kuhn, *Chem. Phys. Lett.*, 1970, **6**, 207–210.

28 V. Czikkely, H. D. Försterling and H. Kuhn, *Chem. Phys. Lett.*, 1970, **6**, 11–14.

29 G. Scheibe, *Angew. Chemie*, 1939, **52**, 331–637.

30 E. S. Emerson, M. A. Conlin, A. E. Rosenoff, K. S. Norland, H. Rodriguez, D. Chin and G. R. Bird, *J. Phys. Chem.*, 1967, **71**, 2396–2403.

31 A. P. Deshmukh, N. Geue, N. C. Bradbury, T. L. Atallah, C. Chuang, M. Pengshung, J. Cao, E. M. Sletten, D. Neuhauser and J. R. Caram, *Chem. Phys. Rev.*, 2022, **3**, 21401.

32 A. V. Buettner, *J. Chem. Phys.*, 2004, **46**, 1398–1401.

33 L. J. E. Hofer, R. J. Grabenstetter and E. O. Wiig, *J. Am. Chem. Soc.*, 1950, **72**, 203–209.

34 G. Oster and Y. Nishijima, *J. Am. Chem. Soc.*, 1956, **78**, 1581–1584.

35 B. Wilhelmi, *Chem. Phys.*, 1982, **66**, 351–355.

36 M. Van der Auweraer, M. Van den Zegel, N. Boens, F. C. De Schryver and F. Willig, *J. Phys. Chem.*, 1986, **90**, 1169–1175.

37 G. G. Stokes, *Philos. Trans. R. Soc. London*, 1853, **143**, 385–396.

38 G. Scheibe, *Angew. Chemie*, 1936, **49**, 563.

39 G. Scheibe, *Angew. Chemie*, 1937, **50**, 212–219.

40 F. Würthner, *Angew. Chem., Int. Ed.*, 2020, **59**, 14192–14196.

41 J. Luo, Z. Xie, J. W. Y. Lam, L. Cheng, H. Chen, C. Qiu, H. S. Kwok, X. Zhan, Y. Liu, D. Zhu and B. Z. Tang, *Chem. Commun.*, 2001, 1740–1741.

42 Y. Hong, J. W. Y. Lam and B. Z. Tang, *Chem. Soc. Rev.*, 2011, **40**, 5361–5388.

43 Y. Chen, J. W. Y. Lam, R. T. K. Kwok, B. Liu and B. Z. Tang, *Mater. Horiz.*, 2019, **6**, 428–433.

44 C. Yu, C. Yu, C. Yu, X. Fang, Q. Wu, L. Jiao, L. Sun, Z. Li, P. K. So, W. Y. Wong and E. Hao, *Org. Lett.*, 2020, **22**, 4588–4592.

45 K. E. Horner and P. B. Karadakov, *J. Org. Chem.*, 2013, **78**, 8037–8043.

46 W. Qin, M. Baruah, M. Van der Auweraer, F. C. De Schryver and N. Boens, *J. Phys. Chem. A*, 2005, **109**, 7371–7384.

47 G. De Belder, S. Jordens, M. Lor, G. Schweitzer, R. De, T. Weil, A. Herrmann, U. K. Wiesler, K. Müllen and F. C. De Schryver, *J. Photochem. Photobiol., A*, 2001, **145**, 61–70.

48 Y. Lee, S. Das, R. M. Malamakal, S. Meloni, D. M. Chenoweth and J. M. Anna, *J. Am. Chem. Soc.*, 2017, **139**, 14733–14742.

49 M. Van der Auweraer, P. Ballet, F. C. De Schryver and A. Kowalczyk, *Chem. Phys.*, 1994, **187**, 399–416.

50 M. N. Berberan-Santos, E. N. Bodunov and B. Valeur, *Chem. Phys.*, 2005, **315**, 171–182.

51 L. Pandey and M. Van der Auweraer, *J. Appl. Phys.*, 2011, **110**, 53712.

52 A. Blumen, J. Klafter and R. Silbey, *J. Chem. Phys.*, 1980, **72**, 5320–5332.

53 A. Blumen and R. Silbey, *J. Chem. Phys.*, 1979, **70**, 3707–3714.

54 S. G. Fedorenko and A. I. Burshtein, *Chem. Phys.*, 1988, **128**, 185–198.

55 G. Zumofen and A. Blumen, *Chem. Phys. Lett.*, 1982, **88**, 63–67.

56 A. Blumen and J. Manz, *J. Chem. Phys.*, 1979, **71**, 4694–4702.

57 J. Huang, F. de Jong, D. M. E. van Raamsdonk, J. Vandenwijngaerden, A. Inoue, D. Escudero, L. Van Meervelt, M. Van der Auweraer and W. Dehaen, *Adv. Opt. Mater.*, 2023, 2301328.

58 B. R. Henry and W. Siebrand, in *Organic molecular photophysics*, ed. J. B. Birks, John Wiley & Sons, London, 1973, vol. 1, p. 186.

59 Y. Yu, Y. Hong, C. Feng, J. Liu, J. W. Y. Lam, M. Faisal, K. M. Ng, K. Q. Luo and B. Z. Tang, *Sci. China, Ser. B: Chem.*, 2009, **52**, 15–19.